CHEMISTRY OF MATERIALS

pubs.acs.org/cm

Article

Probing Electrochemical Mg-Ion Activity in $MgCr_{2-x}V_xO_4$ Spinel Oxides

Bob Jin Kwon, Ka-Cheong Lau, Haesun Park, Yimin A. Wu, Krista L. Hawthorne, Haifeng Li, Soojeong Kim, Igor L. Bolotin, Timothy T. Fister, Peter Zapol, Robert F. Klie, Jordi Cabana, Chen Liao, Saul H. Lapidus, Baris Key,* and John T. Vaughey*

Cite This: *Chem. Mater.* 2020, 32, 1162−1171

Read Online

ACCESS | Metrics & More | Article Recommendations | Supporting Information

ABSTRACT: Mg migration in oxide spinels is impeded by strong affinity between divalent Mg and oxygen, suggesting a necessity of exploring new chemistry of solid lattices for functional Mg-ion electrode materials. Cationic mobility with a suitable activation energy in Cr spinels is evidenced by theoretical and experimental results, while redox potentials of V are appropriate to operate with currently limited candidates of nonaqueous electrolytes. By controlling the structure, composition, and complexity, a largely solid-solution $MgCrVO_4$ spinel was synthesized, which, unlike nanocomposites, can bring together the advantages of each transition metal in the lattice. The spinel was successfully synthesized by a simple solid-state reaction with minor inactive Cr- or V-rich components, which was confirmed via ^{25}Mg MAS NMR and high-resolution X-ray diffraction analyses. A thermally and anodically stable $Mg(TPFA)_2$/triglyme electrolyte was utilized for high-temperature electrochemistry and lowering kinetic barriers at and across interfaces so as to observe intercalation behavior of Mg in the designed lattice. Multimodal characterization confirmed an apparent bulk demagnesiation from $MgCrVO_4$ with partial reversibility by probing evolution of the local and long-range structure as well as vanadium and chromium electronic states within the lattice. Characterization experiments also provided a direct evidence for (de)intercalation reactions that occurred without any major competitive conversion reactions or insertion of protons into the lattice, except for the formation of a surface rock salt phase upon charge. These findings in Mg-ion activity expand opportunities to design Mg spinel oxide materials while highlighting the need to identify the origins of reversibility challenges due to, but not limited to, phase stability, particularly for the charged states, barriers at the interface, electrolyte stabilities, and desolvation phenomena, collectively hindering practical use as cathode materials.

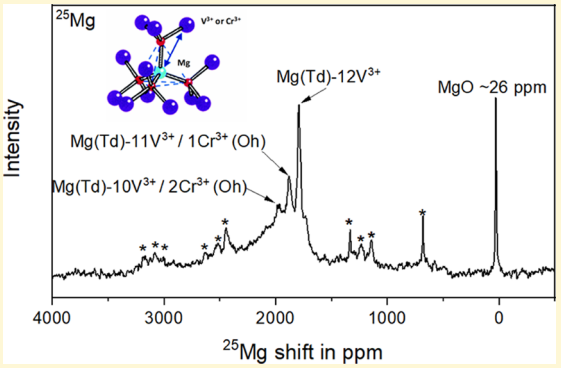

INTRODUCTION

Rechargeable magnesium-ion batteries that are paired with a metallic Mg anode have been considered as an alternative to current Li-ion technology due to their theoretically high capacity, low cost, and safety.[1−3] Realistic prospects of such an electrochemical system strongly rely on the properties of a cathode material, which determines both redox potentials and the amount of reversible charge supplied by structural activity in the solid lattice as the anode reaction has already been demonstrated on the Mg metal with certain electrolytes.[4,5] Since the Mo_6S_8 Chevrel phase was reported by Aurbach et al. in 2000, reversible Mg intercalation has only been achieved by classes of transition metal sulfides, allowing a facile diffusion.[6,7] However, these compounds operate at low potentials (~1 V vs Mg/Mg^{2+}) with restricted energy stored in the battery, which limits practical applications.[7−9] Enhanced redox potentials and energy densities can theoretically be obtained if the soft anions are replaced by oxygen,[10] which, at the same time, increases barriers for Mg^{2+} mobility, considering electronegativity of the anions and oxophillicity of Mg^{2+}.[11] Conversion reactions and/or high barriers of desolvation at the electrode−electrolyte interfaces are dominant when the driving force does not reach the activation energy for diffusion.[12−15] From a computational study, spinel structures are expected to provide feasible integration of operational potential, capacity, and cation mobility since the lattice allows for a relatively facile ion transport through three-dimensional diffusion pathways.[10] Feasibility of Mg^{2+} intercalation into Mn_2O_4 spinel was reported experimentally.[16,17] However, Mg^{2+} mobility in the Mn spinel lattice is still nonideal, with predicted ~0.8 eV activation energy from theory.[10]

Received: October 14, 2019
Revised: December 26, 2019
Published: December 27, 2019

Recently, theoretical calculations have incorporated screening on the potential, capacity, thermodynamic structure, and ionic mobility of the spinel candidates with various transition metals paired with Mg^{2+}.[10] Among various spinels, $MgCr_2O_4$ satisfies relatively the facile mobility of Mg^{2+} with the activation energies for a Mg^{2+} hop to an adjacent vacant site as low as ~0.6 eV from both density functional theory (DFT) calculations and solid-state nuclear magnetic resonance (NMR) experiments.[18,19] However, the redox potentials for Mg^{2+} (de)intercalation (~4.2 V vs Mg/Mg^{2+}) preclude the possibility of $MgCr_2O_4$ as a functional electrode when assembling with the current state-of-the-art electrolytes,[4,20] which limit the upper voltage to ~3.5 V versus Mg/Mg^{2+}, where electrolyte degradation and decomposition dominate.[18−21] Furthermore, instability of Cr^{+4} is another challenge in utilizing Cr redox chemistry. On the other hand, the oxidative potential of vanadium (~3.4 V vs Mg/Mg^{2+}) is comparatively lower than chromium, which enables the use of current electrolytes without significant decomposition or chemical degradation. Currently, no report exists on Mg migration activity in vanadium spinels, including our unsuccessful attempts to demagnesiate MgV_2O_4.[10]

The shortcomings of Cr and V spinels can be mitigated by combining the transition metals intimately in a $MgCrVO_4$ lattice. Herein, we demonstrate moderate Mg^{2+} mobility with a suitable potential in $MgCrVO_4$, a solid-solution spinel oxide, when paired with a Mg metal anode in a thermally and anodically semistable nonaqueous electrolyte. Theoretical prediction of Mg migration behavior supports the hypothesis by indicating that Mg activation energy is preserved when introducing V into a Cr oxide spinel lattice in a form of solid solution. The complex structure was examined via high-resolution synchrotron X-ray diffraction (HR-XRD) and solid-state nuclear magnetic resonance (SS-NMR), which provides a direct evidence of the solid-solution nature of the Mg^{2+} environment. The structural/electrochemical activity relationship was examined via HR-XRD, SS-NMR, scanning transmission electron microscopy (STEM), X-ray absorption spectroscopy (XAS), and ICP-OES. A significant portion (up to ~0.7 moles by semiquantitative ^{25}Mg MAS NMR) of Mg^{2+} was deintercalated electrochemically from the spinel lattice. Structural distortion and electronic evolution of redox metals suggest clear Mg activity throughout the bulk spinel oxide frame. An oxidative potential plateau at ~3.25 V with a charge capacity of ~100 mAh/g was observed in a coin cell, consistent with the $V^{3+/4+}$ redox. Partial reversibility was achieved with ~80 mAh/g discharge capacity with an apparent 0.15 Mg^{2+} insertion when lowering potential to 0.25 V (vs Mg/Mg^{2+}), currently hindering the use of the material as a practical cathode. The observation of a rock salt phase formation on the surface upon demagnesiation would be one of the possible origins to explain partial reversibility, high polarization, and hysteresis of the electrochemical reactions. Even though completely reversible reactions were not accomplished in the given electrochemical configuration, and in the context of nonideal electrolytes currently available for such high voltage spinel oxides, these results have the potential to open a new avenue for new Mg^{2+} intercalation compounds.

RESULTS AND DISCUSSION

Insight into migration behavior of Mg^{2+} in the designed $MgCrVO_4$ was obtained from first-principle DFT calculations in the dilute vacancy limit to show an effect of vanadium introduction into $MgCr_2O_4$ (Figure 1). The diffusion pathway in the spinel (T_d-O_h-T_d) goes through the triangular face

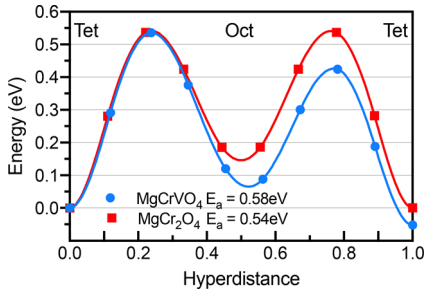

Figure 1. Minimum energy pathways for Mg migration in $MgCr_2O_4$ and $MgCrVO_4$ at the dilute vacancy limit.

shared between the stable and intermediate sites, showing a typical hill-shaped energy profile. The calculated activation energy of Mg migration reflects a potential activity of Mg in the cathode lattice at the initial stage of discharge. The predicted barriers for a Mg hop in the spinel structure are 0.58 eV for $MgCrVO_4$ and 0.54 eV for $MgCr_2O_4$ (Figure 1). The similar hopping barrier in the Cr-V solid-solution phase compared to a $MgCr_2O_4$ single B-site spinel indicates facile migration of Mg^{2+} in the lattice, supporting our assumption that the designed chemical composition reduces voltage into the electrolyte stability range while not inhibiting Mg mobility.

$MgCrVO_4$ spinel was synthesized by a simple solid-state reaction in a stoichiometric ratio of Mg/Cr/V in an inert atmosphere. Electrochemical tests of the synthesized spinel for NMR measurements were carried out in a Swagelok cell at 110 °C with a composite cathode, consisting of 60% of an active spinel oxide and 40% of conductive carbon with a total mass of ~50 mg and a Mg foil as an anode. All electrochemical tests were conducted in a nonaqueous Mg electrolyte containing $Mg(TPFA)_2$ salt dissolved in triglyme. The electrolyte exhibits a high anodic stability of up to ~4.0 V (Mg/Mg^{2+}) with mitigated cathodic decomposition.[22] Furthermore, thermal gravimetric analysis of the $Mg(TPFA)_2$ salts revealed its stability of up to 150 °C without sublimation, enabling electrochemical tests at high temperature (Figure S1). The potentials presented in the data were referenced to the Mg/Mg^{2+} redox couple throughout this manuscript. The cathode powder (50 mg) consisting of carbon and active oxide was charged to 3.8 V at a constant current (~C/70) and held at 3.8 V versus Mg/Mg^{2+} until ~150 mAh/g charge capacity was reached (Figure 2a). It is worth noting that the designed configuration of the cell is intended mainly for NMR characterization with large areal cathode loading; therefore, electrochemical response is considered as secondary. Since the predicted potential of demagnesiation in a $MgCr_2O_4$ spinel is around 4.2 V (vs Mg/Mg^{2+}),[19] which is out of the stability window of the electrolyte, presumably only the redox of vanadium in the solid solution was utilized at the applied potentials. Subsequent electrochemical reintercalation of Mg^{2+} was performed by applying a constant current at ~C/70 to 0.25 V, showing a cathodic plateau at ~0.5 V with ~100 mAh/g discharge capacity (Figure 2a).

High-resolution X-ray diffraction was measured from the spinels at different states of charges to gain insight into the structural evolution such as contraction or expansion of lattice and/or symmetrical alteration of the geometry as a response to

https://dx.doi.org/10.1021/acs.chemmater.9b04206
Chem. Mater. 2020, 32, 1162−1171

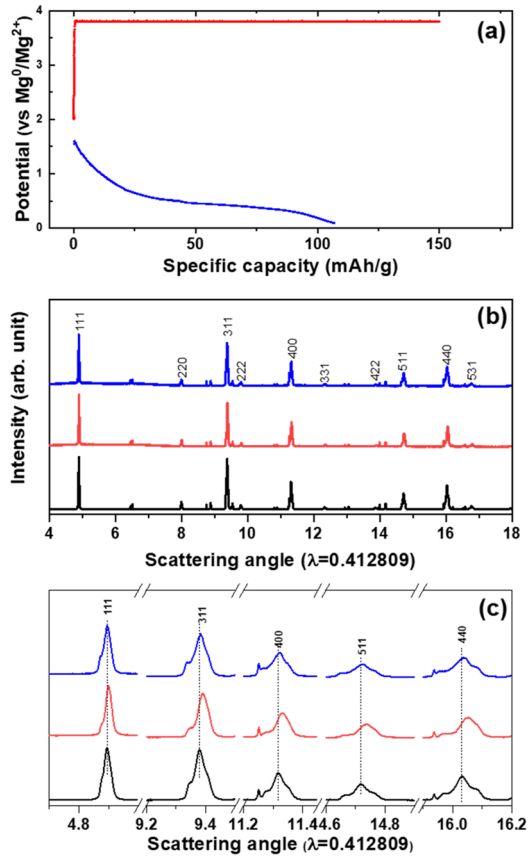

Figure 2. (a) Representative potential versus capacity profiles of spinel $MgCrVO_4$ measured in a Swagelok cell at 110 °C paired with a Mg foil anode. The cell was charged to 3.8 V at a constant current and held at this constant potential to 150 mAh/g and then discharged to 0.25 V at a constant current. (b, c) High energy X-ray diffraction patterns of the corresponding pristine (black), charged (red), and discharged electrode powders (blue) in (b) wide and (c) magnified scattering angles.

electrochemical treatment (Figure 2b,c). Detailed Rietveld refinement showed that the pristine material consisted of mainly a cubic spinel structure ascribed to $MgCrVO_4$ with lattice parameters in between that of $MgCr_2O_4$ and MgV_2O_4, along with minor components assigned to a vanadium-rich $MgCr_{2-x}V_xO_4$ (~10%), $MgCr_2O_4$ (~17%), Cr_2O_3 (~6%), V_2O_3 (~3%), and MgO (~3%) produced in the solid-state reaction at the calcination temperature (Figure S2). Each spinel phase was refined with different lattices and structural parameters; however, due to the insensitivity of X-rays of the difference between V^{3+} and Cr^{3+}, the composition was induced by the difference of ionic radius of V^{3+} and Cr^{3+} in the oxides (Table 1). Diffraction of the charged electrode after ~150 mAh/g charge capacity showed that the peaks were shifted to higher angles in all planes of the cubic system as compared to the pristine state, suggesting a decrease of the unit cell volume along with oxidized states of vanadium (Figure 2c). Interestingly, the contraction of lattice was mainly observed in the main $MgCrVO_4$ spinel phase (Table 1). A visible decrease in the ratio of intensity between the (111) and (311) reflections was observed, depending on the occupancy of Mg^{2+} in the tetrahedral site, inducing a distortion of the structure (Figure S3). This result is consistent with XRD of $MgCr_2O_4$ demagnesiation previously reported.[18] However, due to the relatively weak scattering of Mg^{2+} and the overlapping phases, refinement of precise values of the Mg^{2+} occupancy was unreliable; however, the trend of Mg^{2+} occupancy suggests significant demagnesiation. Upon remagnesiation with ~100 mAh/g discharge capacity, all diffraction peaks largely reverted to the original positions, indicating an increase of lattice volume. The long-range structural reversibility of the spinel suggests Mg reactivity throughout the bulk oxide frame, while the lack of new phases or evidence of amorphization suggests that no secondary phases were formed via conversion reactions.[12]

Table 1. Lattice Parameters of Phase Components (in Å) in Pristine, Charged, and Discharged Cubic $MgCrVO_4$ Phase Components[a]

state of charge	$MgCrVO_4$	$MgCr_2O_4$	V-rich $MgCr_{2-x}V_xO_4$
pristine	8.373	8.347	8.403
charged	8.363	8.345	8.402
discharged	8.371	8.346	8.404

[a]The values indicate a parameter in a cubic spinel lattice.

The nature and changes of the Mg^{2+} local environment in the spinel oxides were studied by solid-state ^{25}Mg MAS NMR (Figure 3). The spectra provides Fermi contact Mg shifts

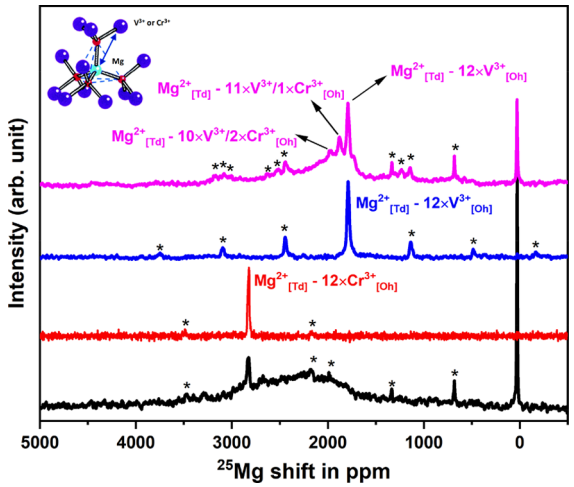

Figure 3. ^{25}Mg magic angle spinning (MAS) NMR spectra of $MgCrVO_4$ (black), $MgCr_2O_4$ (red), MgV_2O_4 (blue), and V-rich $MgCr_{0.4}V_{1.6}O_4$ (magenta) spinel. Asterisk marks indicate spinning sidebands.

depending on the ensemble of first and second coordination shell Mg-O-Cr/V connectivity in the lattice due to the presence of paramagnetic centers at $Cr^{3+}$and V^{3+}.[23,24] The spectra of pristine material showed a broad feature between ~1500 and ~3500 ppm with a center of mass at ~2300 ppm due to lattice Mg^{2+} (Figure 3).[24] As compared with the sharp peaks of MgV_2O_4 (~1800 ppm) and $MgCr_2O_4$ (~2800 ppm) spinel spectra, the broad and largely Gaussian resonance centered at ~2300 ppm indicates a solid-solution distribution of Mg/Cr-V in the lattice (Figure 3 and Figure S4). The peak profile is consistent with NMR studies of materials with random transition metal ordering in the lattice such as in $Li[Ni_xMn_xCo_{(1-2x)}]O_2$ (x = 1/3)-layered cathode materials in Li-ion or in $MgMnO_2$ rock salt lattice with random Mg and Mn ordering, that is, solid solutions.[25,26] The broad resonance was accompanied by a sharp signal at ~2800 ppm, which could

https://dx.doi.org/10.1021/acs.chemmater.9b04206
Chem. Mater. 2020, 32, 1162−1171

be assigned as Mg^{2+} in locally segregated Mg-Cr-O spinel domains, which was also detected in HR-XRD analysis. A shoulder in the Gaussian line shape is also observed on the low frequency side, centered around 1800 ppm, which could be due to the presence of a minor MgV_2O_4-like local order. However, since no distinct resonance was observed, this phase and the 10% impurity detected in the HR-XRD are ascribed to a V-rich $MgCr_{2-x}V_xO_4$.[24] A V-rich composition ($MgCr_{0.4}V_{1.6}O_4$) was also prepared to verify this and to explore the feasibility of preparing a material with more electrochemically active vanadium (Figure S4). The ^{25}Mg spectra of $MgCr_{0.4}V_{1.6}O_4$ (Figure 3 and Figure S5) showed a gradual distribution with an asymmetric shape of lattice Mg coordinated to V-rich domains. In the spinel structure, one Mg^{2+} in the tetrahedral site is coordinated with 12 Cr/V in octahedral sites through oxygen anions. Since the degree of shift of ^{25}Mg resonance is proportional to the number of coordinations of Cr and V, clear paramagnetic resonances at ∼1800, ∼1884, and ∼1968 ppm corresponding to the local domains of Mg coordinated to $12V^{3+}$, $11V^{3+}/1Cr^{3+}$, and $10V^{3+}/2Cr^{3+}$, respectively, were detected (Figure 3 and Figure S5), whereas the coordination expected for $9V^{3+}/3Cr^{3+}$ at ∼2052 ppm was barely observed. These observations are consistent with random distribution of Cr within the V-rich spinel lattice. Furthermore, the spectrum with an absence of $MgCr_2O_4$ resonance at ∼2800 ppm supports Cr-V miscibility for $MgCr_{0.4}V_{1.6}O_4$ (Figure 3 and Figure S5). A sharp diamagnetic resonance at ∼26 ppm was observed due to minor MgO from the synthesis, which was also detected in HR-XRD of $MgCrVO_4$.[26]

The ^{25}Mg spectra enabled analysis of lattice Mg^{2+} in a semiquantitative manner. It is worth noting that ^{25}Mg is low gamma, quadrupolar nuclei, implying that there is an uncertainty of errors in any quantification due to various effects due to, but not limited to, relaxation and magnetism. Herein, we show normalized intensity comparisons only for the paramagnetic resonances corresponding to the lattice Mg content, reflecting a degree of deintercalation of Mg. The charged oxide ^{25}Mg NMR spectrum (Figure 4) showed a major loss of intensity in the main paramagnetic resonance along with a shift of gravimetric center to lower frequencies by

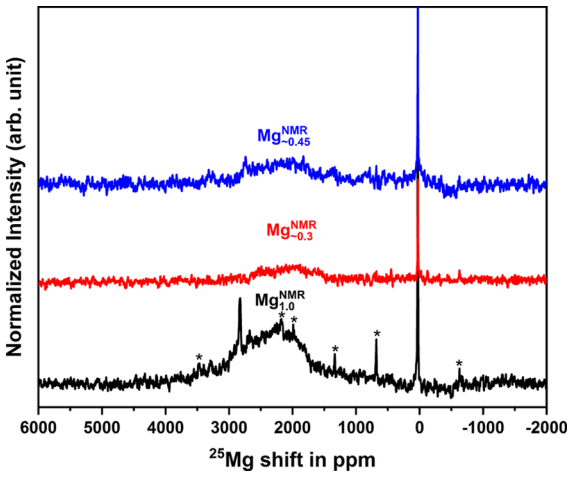

Figure 4. Semiquantitative ^{25}Mg magic angle spinning (MAS) NMR spectra of pristine (black), charged (red), and discharged (blue) spinel oxides. All spectra were normalized. Asterisk marks indicate spinning sidebands.

∼250 ppm due to an oxidation of V and/or Cr via an apparent electrochemical deintercalation of lattice Mg^{2+}, consistent with HR-XRD observations.[18] The normalized resonance spectra of charged spinel indicated that up to ∼0.7 mol Mg^{2+} were deintercalated from the lattice, consistent with the HR-XRD results of significant demagnesiation. Another strategy to quantify lattice Mg^{2+} for the ex situ samples was attempted by inductively coupled plasma measurements (via ICP-OES). A decrease in the Mg^{2+} content upon charge reaction and a subsequent increase in the Mg^{2+} content upon discharge reaction were observed. Unfortunately, unreliable Mg to transition metal ratios were obtained possibly due to issues with fully dissolving the composite electrodes with carbon in solutions, an inherent problem associated with Cr-bearing solid oxides and/or residues of Mg-electrolyte species, revealing a limit of reliable quantification via ICP (Table S1). In ^{25}Mg NMR spectra of the charged state, the disappearance of the $MgCr_2O_4$ signal at 2800 ppm was observed, despite the fact that the cell never reached the oxidative potential of Cr^{3+} (∼4.2 V vs Mg/Mg^{2+}). Possible explanations could be internal migration of Mg within the oxide analogous to Li migration in layered oxide battery materials upon delithiation[27,28] or that the elevated temperature electrochemical testing conditions enable some Cr redox at the lower potentials. To probe the existence of the latter possibility, another cell was charged at a constant potential of 3.6 V until ∼150 mAh/g charge capacity was reached (Figure S6a) to probe the effect of a lower voltage cutoff. A substantial change in the intensity ratio of the (111) and (311) reflections using a conventional diffractometer was observed in XRD (Figure S6b), confirming structural activity, whereas the NMR (Figure S6c) showed a reduced intensity change versus pristine and ∼0.4 mol Mg ions removed from the lattice. The results suggest that the upper cutoff potential has some role in controlling the incorporation of Cr redox activity. It must be noted that the increased Mg removal capacity beyond V redox may have significant phase stability issues since the electrochemically charged state of $MgCr_2O_4$ was reported to be unstable.[18] It is also possible that, due to the broad nature of the peaks and insensitivity of ^{25}Mg NMR, the semiquantitative results could be overestimating the amount of Mg removed from the lattice up to 30%.

To probe the element-specific redox behavior of the transition metal, X-ray absorption spectroscopy was utilized (Figure 5). X-ray absorption near edge spectroscopy (XANES) and extended X-ray absorption fine structure (EXAFS) are specific probes of local atomic and electronic structure and can potentially provide the necessary information to understand the electronic evolution of the transition metals surrounding the Mg ion at different states of charges.[29,30] Therefore, the absorption spectra provides the oxidation states of redox-active metals.[16] The spectra of the charged spinel revealed a shift of the V K-edge to a higher energy, by roughly 0.7 eV, as compared to the pristine state (∼5485.5 eV) due to the oxidation of the vanadium sites by a removal of Mg^{2+} (Figure 5a). In addition, a pre-edge peak at ∼5468.5 eV was also observed, consistent with a weakening of centrosymmetric coordination commonly found in V^{4+} and V^{5+} compounds. This increase in local disorder is also present in the extended X-ray absorption fine structure, which shows a systematic decrease in the Fourier-transformed fine structure ($|\chi(R)|$; Figure 5b). The slight increase of disorder is also consistent with partial amorphization in the demagnesiated oxide; however, both the near edge and extended fine structure

https://dx.doi.org/10.1021/acs.chemmater.9b04206
Chem. Mater. 2020, 32, 1162−1171

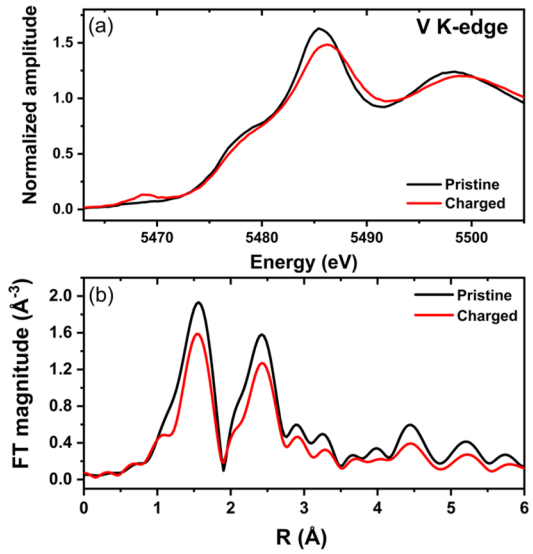

Figure 5. (a) V K-edge X-ray absorption spectra and (b) the corresponding extended X-ray absorption fine structure of pristine and charged spinel $MgCrVO_4$ prepared in a Swagelok cell at 110 °C.

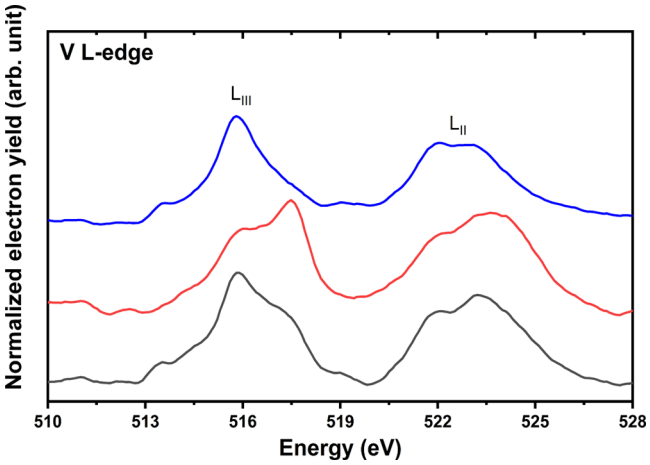

Figure 6. V L-edge X-ray absorption spectra of pristine (black), charged (red), and discharged (blue) $MgCrVO_4$ prepared in a Swagelok cell at 110 °C.

suggest an apparent transition from a cubic to a partially distorted structure upon removal of Mg^{2+}, which is consistent with the diffraction analysis. On the other hand, no changes of the Cr K-edge main edge at ∼6009.7 eV were detected upon demagnesiation likely due to the fact that the predicted oxidation potential of Cr in the spinel was never reached in the electrochemical experiment (Figure S7). Another possibility for the lack of changes in the Cr K-edge result is that the oxidized Cr was unstable and degraded rapidly, a phenomenon reported previously for $MgCr_2O_4$ and discussed above in the NMR results.[18]

The structural reversibility and Mg intercalation into the demagnesiated lattice was further explored via semiquantitative ^{25}Mg NMR. The spectrum of an electrode charged (to 3.8 V) and then discharged at a constant current to 0.25 V with ∼100 mAh/g discharge capacity showed an increase of intensity in the paramagnetic ^{25}Mg resonance(s), while the center of the mass of the resonance(s) was slightly shifted to a higher frequency (Figure 4). Approximately 0.15 mol Mg ions were estimated to be intercalated back into the lattice based on the ^{25}Mg analysis along with a reemerged resonance at ∼2750 ppm, possibly due to reformation of a $MgCr_2O_4$-like order (Figure 4).

Observation of partial reversibility from ^{25}Mg quantification was further investigated by soft XAS measurements on a V L-edge environment. V L-edge spectra were collected in a total electron yield mode, which is sensitive to ∼5 nm depth, providing the chemical states of V at the surface.[31] The L_{III} and L_{II} edges are generated by electronic transition to the 3d band from the $2p_{1/2}$ and $2p_{3/2}$ levels, respectively.[32] The changes in the multiplet structure are attributed to the variation of symmetry of the ground state, whereas the chemical shift reflects alteration of the formal valence states of V.[31,32] As shown in Figure 6, the V L_{III} edge spectra of pristine $MgCrVO_4$ presented intense absorption features at ∼515.8 and ∼517.5 eV, which could be associated with the existence of dominant V^{3+} with minor V^{4+} on the surface. Upon demagnesiation, the center of gravity of the spectra clearly shifted to higher absorption energy with the intensified V^{4+} peak, indicating a clear oxidation of vanadium. On the subsequent cathodic reaction, the features of spectra were reverted to original positions, including some evidence for slightly more reduced states than the pristine. A reversible redox reaction at V was observed on the surface at least which is consistent with the observation of partial reversibility of Mg^{2+} intercalation.

The XAS results, coupled with observations from HR-XRD suggest partial reversibility with ∼100 mAh/g discharged capacity accounting for 0.15 mol Mg, as opposed to a theoretical 0.35 mol Mg. Other intercalating species, such as H^+ formed due to decomposition of solvent molecules in the electrolyte by being exposed to high temperature and voltage, may explain the additional capacity. To probe such a phenomenon, a deuterated diglyme solvent was used in the electrolyte formulation for solid-state ^2H MAS NMR measurements that can detect lattice protons (Figure 7).[33,34] No paramagnetic deuterium resonances were detected in the discharged oxide, and only deuterated diglyme/SEI protons showed a strong signal at ∼3 ppm, consistent with the absence of lattice protons (Figure 7).[35] Diamagnetic ^{25}Mg resonance at 26 ppm due to MgO was also found to undergo changes in intensity upon charge and discharge (Figure S8), although the

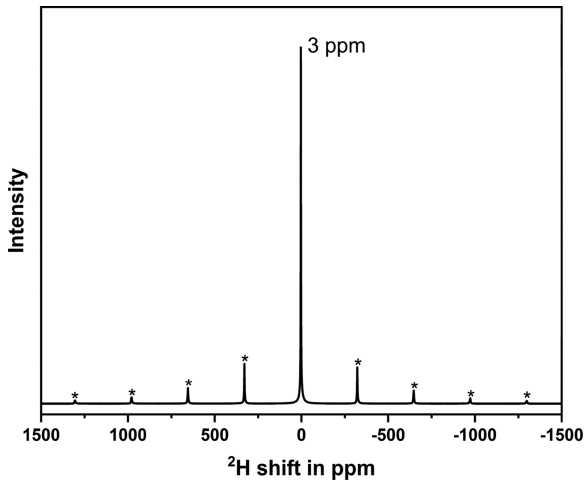

Figure 7. ^2H MAS NMR for discharged $MgCrVO_4$ prepared in an electrolyte of $Mg(TPFA)_2$ dissolved in a deuterated diglyme.

https://dx.doi.org/10.1021/acs.chemmater.9b04206
Chem. Mater. 2020, 32, 1162−1171

mechanism for the changes is not yet well understood. Interestingly, a new resonance centered around 0 ppm was observed after the discharge, which could be related to a diamagnetic Mg-bearing species buildup in the electrode at low voltage and may be correlated to the additional capacity. To observe possible formation of Mg chemical species on the surface and/or at the interface of solid/electrolyte, X-ray photoelectron spectroscopy (XPS) was performed (Figure S9). The electrochemically harvested composite electrodes showed surface/SEI buildup, possibly due to electrolyte oxidation and changes in intensities of Mg 2s and 2p binding energies upon charge and subsequent discharge, consistent with Mg activity observed in ^{25}Mg NMR analysis. The surface buildup observed in the charged sample may be associated with the onset of impeded transport at the interface and could be contributing to partial reversibility of Mg activity upon one full cycle.

The feasibility of a traditional full cell configuration using a $MgCrVO_4$ cathode was explored via an electrochemical performance test carried out in a coin cell at 110 °C. The positive electrode consisted of active $MgCrVO_4$, a conductive carbon, and binder with 6:2:2 ratio in mass, casted onto a stainless steel mesh. The cell was galvanostatically charged to 3.8 V and discharged to 0.25 V at a rate of ∼C/70 (Figure 8).

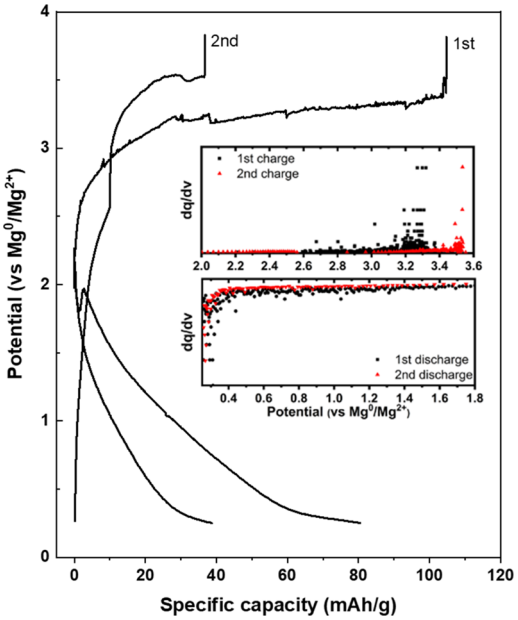

Figure 8. Representative potential versus specific capacities of spinel $MgCrVO_4$ measured in a potential window of 0.25−3.80 V (vs Mg/Mg^{2+}) at 110 °C in a coin cell paired with a Mg foil anode. The insets are dq/dv curves of the corresponding reactions.

An anodic applied current resulted in a plateau at ∼3.25 V with an inflection point at ∼3 V. A total charge capacity of ∼100 mAh/g was observed, corresponding to ∼0.35 mol Mg^{2+} removed from the spinel lattice, assuming maximum Coulombic efficiency. Once the potential reached ∼3.4 V with ∼100 mAh/g, the potential sharply spiked, and the 3.8 V cutoff was reached with no further charging. In the subsequent discharge cycle, a cathodic reaction proceeded from ∼2 V with a gradual decrease in potential. A capacity of ∼80 mAh/g was achieved at a lower voltage cutoff of 0.25 V. In the second full cycle, the charge capacity and subsequent discharge capacities dropped to ∼40 mAh/g, and the large redox potential hysteresis between the cathodic and anodic reactions increased to over 2.5 V (Figure 8). The third cycle is not shown due to negligible capacities obtained, that is, cell death. The spinel oxide was also tested in an alternative electrochemical system, consisting of $Mg(ClO_4)_2$ dissolved in propylene carbonate paired with a carbon reference at 50 °C (Figure S10). A similar anodic reaction was observed up to 1.4 V (vs carbon), corresponding to ∼3.4 V in a full cell, whereas a significantly lower reversibility upon cathodic reaction was down to −1.4 V (vs carbon), corresponding to ∼0.5 V in a full cell, which could suggest the role temperature for facile Mg dynamics at the interface and in the bulk. The results, while consistent with the structural Mg activity, clearly point out to other phenomena as origins for the partial reversibility hindering the practical use of the material as a cathode.

To track any possible origin of significant polarization between the anodic and cathodic reactions, aberration-corrected scanning transmission electron microscopy was performed. Activation of Mg migration in the spinel lattice required a high oxidation potential at raised cell temperature, possibly generating surface reconstruction due to highly oxidized electrolyte species.[21] As shown in Figure 9, a formation of rock salt was observed on the surface of the demagnesiated oxide with the [001] zone axis, whereas well-crystalline spinel lattices were presented in both the bulk and surface of pristine $MgCrVO_4$. The corresponding FFT supported the local transformation of spinel to rock salt on the surface (Figure 9). Detailed mechanism of the interfacial reaction is unclear as of now, but the presence of the rock salt phase on the surface might impede ion transport at the interface upon remagnesiation, which could result in formation of additional Mg-bearing diamagnetic species observed in NMR, polarization, and partial reversibility in the electrochemistry.

At this point, it is critically important to identify the origin(s) of reversibility challenges in the system to be able to move forward. To elaborate, in this study, we have identified a relatively stable charge state for oxidized vanadium relative to chromium. However, any metastability or self-discharge mechanism reducing the charged redox state was not explored in detail and will be the focus of a future in situ characterization study. Furthermore, the effects of surface/interfacial species such as the rock salt phase, organic/electrolyte decomposition buildup, and insulating MgO impurities detected are not clear. Interfacial barriers to ion transport, particularly during remagnesiation, can be a key issue; therefore, surface-specific studies can be of great interest in the future. While magnesium electrolyte stability at high voltages (and temperatures) and detrimental effects on electrochemical performance can never be ruled out, the magnesium solvation structure at the oxide−electrolyte interface and kinetic barriers in desolvation phenomena, in general, could be playing a critical role in limiting remagnesiation of the lattice.

CONCLUSIONS

$MgCrVO_4$, with the general composition $MgCr_{2-x}V_xO_4$ ($0 \le x \le 1.6$) was synthesized. The Mg^{2+} mobility in the structure was examined via DFT calculation, and the complexity in the structure was probed by diffraction, NMR, XAS, and electrochemical characterization, providing direct evidence of a Cr-V solid solution within the lattice and its bulk Mg activity. Significant electrochemical demagnesiation was observed

https://dx.doi.org/10.1021/acs.chemmater.9b04206
Chem. Mater. 2020, 32, 1162−1171

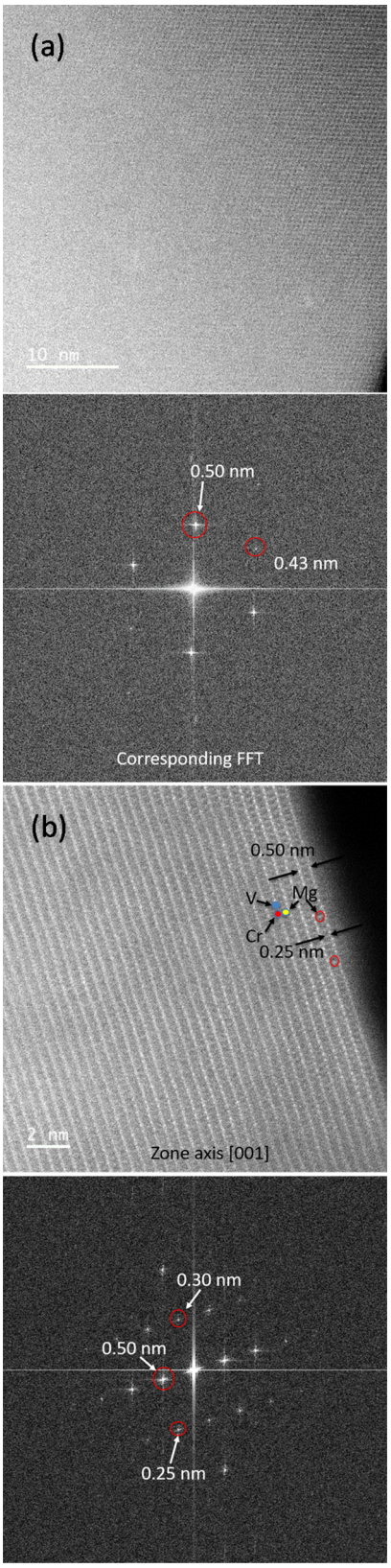

Figure 9. HAADF images (above) and corresponding FFT (below) of (a) pristine and (b) charged $MgCrVO_4$ prepared at 110 °C in a coin cell paired with a Mg foil.

without conversion reactions followed by partial reinsertion of Mg^{2+} in a full Mg-ion cell at a raised temperature. In full cell configuration, hysteresis and low Coulombic efficiency severely limits reversibility of electrochemical reaction and currently hinders any practical use as a cathode material. While no discernible proton insertion was detected that could limit a degree of remagnesiation of the lattice, a surface rock salt phase formation upon demagnesiation was observed, which should shift a focus to possible culprits such as phase stabilities, interfacial barriers, and Mg-ion desolvation phenomena as well as stability issues with nonaqueous Mg-ion electrolytes. Higher usable energy densities of vanadium-rich compositions and exploration of other transition metal compositions with apparent phase stabilities and similar solid-solution structures within these spinel classes will be the logical focus of follow-up studies. The findings reported here enable new strategies for designing functional multivalent electrode materials and aid in identifying key issues with future full cell development using spinel oxides.

METHODS

Synthesis. The synthesis of solid-solution $MgCrVO_4$ was performed through a ceramic high-temperature method. Magnesium hydroxide, vanadium(III) oxide, and chromium(III) nitrate were mixed together in a stoichiometric ratio of 1:1 and heated to 950 °C for 24 H under Ar. $MgCr_2O_4$, MgV_2O_4, and $MgCr_{0.4}V_{1.6}O_4$ were synthesized by a sol–gel-type synthetic route. The desired metal precursors were added in a stoichiometric ratio to 200 mL of deionized water. The total concentration of ions in the solution was 0.025 mol. Citric acid was added to the solution at a 1:1 ratio to the total metal ion concentration. The solution was heated on a hot plate in a fume hood until all water had evaporated. The resultant solutions were calcined at 950 °C in air, 5%H_2/95%Ar, and 3%H_2/97%Ar for $MgCr_2O_4$, MgV_2O_4, and $MgCr_{0.4}V_{1.6}O_4$, respectively. Details of synthetic routes are indicated in Table S2.

A $Mg(TPFA)_2$ ($[TPFA]^-$ = $Al\{OC(CF_3)_3)\}_4^-$) electrolyte for high-temperature electrochemical testing was synthesized by following a recently reported literature method.[22] A 0.1 M electrolyte was prepared by dissolving $Mg(TPFA)_2$ in a triglyme, and then, the solvated THF species were removed at 55 °C under 50 mTorr overnight. Thermogravimetric analysis was carried out to assess the thermal stability of the salt using a PerkinElmer Pyris 1 TGA analyzer.

Characterization. Theoretical values of average cell potentials and Mg migration barriers of $MgCr_2O_4$ and $MgCrVO_4$ were obtained from density functional theory calculations as implemented in the Vienna Ab initio Simulation Package (VASP).[36,37] The core-valence electron interactions were treated using the projector augmented wave (PAW)[38] potentials. The exchange-correlation functionals were described by the generalized gradient approximation (GGA) method developed by Perdew–Burke–Ernzerhof (PBE).[39] A Hubbard U correction[40] was also added to describe the localization of d-electrons of redox-active species, Cr (U = 3.7 eV) and V (U = 3.25 eV).[41] The average cell potential was calculated from the energy difference between the charged and discharged phases. The Mg migration barriers are calculated by the nudged elastic band (NEB) method,[42] where a 2 × 2 × 2 supercell of the primitive cell was used to avoid fictitious interactions between periodic images of diffusing atoms. The V atom distribution in the spinel structure was chosen using the pymatgen code[43] to minimize the electrostatic energy of the cell. The energies at the initial and final states for $MgCrVO_4$ in Figure 1 are not identical because the diffusing Mg atom is coordinated by a different number of Cr and V atoms. The NEB calculations are performed with GGA functional without U correction, as suggested in ref 10.

In this study, two types of cells were used to measure the electrochemical properties of the spinel oxides: Swagelok stainless steel cells and coin cells. For the Swagelok cell tests, spinel oxide powder as a cathode was mixed with Timcal C45 carbon in a 60/40 mass ratio and drop-cast onto 1.5″ in diameter stainless steel current collectors (~30 mg of active material). The electrode powders were placed in Swagelok-type stainless steel cells with a glass fiber separator (Sigma-Aldrich), Mg metal counter electrode (Mg metal foil, purity

https://dx.doi.org/10.1021/acs.chemmater.9b04206
Chem. Mater. 2020, 32, 1162–1171

99.9%, Sigma-Aldrich), and 0.1 M $Mg(TPFA)_2$ electrolyte. For the coin cells, the electrode slurries were prepared by mixing active oxides and Timcal C45 carbon in a 6 wt % binder solution consisting of polyvinylidene difluoride (PVDF; Solvay) in *N*-methylpyrrolidone (NMP; Sigma-Aldrich) to a total of 60:20:20 wt % of oxide, conductive additive, and binder, respectively. The slurry was cast onto a stainless steel mesh with a diameter of 0.5 in. and dried under vacuum at 80 °C overnight to evaporate NMP moieties. The coin cell was assembled in an argon-filled glovebox with the prepared cathode, a Mg metal anode, and a glass fiber separator, where the level of water and oxygen contents was ≤1.0 ppm. Electrochemical measurements of both types of cells were performed using a MACCOR battery cycler at 110 °C. The charge/discharge cutoff potentials were selected to be 3.8/0.25 and 3.6/0.5 V with galvanostatic or potentiometric charge/discharge, depending on the measurement. All potentials in this report are referenced to the redox Mg/Mg^{2+} couple. A rate, C/n, was defined as the current density required to achieve a theoretical capacity of a $MgCrVO_4$ structure, C = 140 mAh/g, in n hours, which was estimated by dividing a theoretical capacity of MgV_2O_4 in half.

High-resolution X-ray diffraction (HR-XRD) was carried out at beamline 11-BM of the Advanced Photon Source (APS) at Argonne National Laboratory (ANL) with an X-ray wavelength of 0.412809 Å. Samples were loaded in Kapton capillaries (0.9 mm diameter), sealed by epoxy glue, and mounted on bases provided by the APS at Argonne National Laboratory. Sample loading procedures were carried out in a glovebox for the XRD measurement. The data points were collected at room temperature with a step size of 0.001° 2θ and a scan rate of 0.01°/s. All diffraction plots are presented in 2θ, where $Q = [4\pi \sin(\theta)]/\lambda$. Powder X-ray diffraction in the Supporting Information was performed on a Bruker D8 Avance using Cu Kα (λ_{avg} = 1.5418 Å) radiation. Scan rates were 0.04° s^{-1} from 15 to 70° (2θ). Rietveld refinements were performed in TOPAS v5.

Solid-state ^{25}Mg magic angle spinning (MAS) NMR experiments were performed at 11.7 Tesla (500 MHz) on a Bruker Avance III spectrometer, operating at a Larmor frequency of 30.64 MHz using a 3.2 mm MAS probe. The spectra were acquired at a spinning speed of 20 kHz for 3.2 mm rotors with a rotor synchronized spin-echo experiment (90°-τ-180°-τ), where τ is 1/r. To ensure quantification in normalized intensity experiments, single-pulse experiments (data not shown) with recycle delays of 0.1−1 s were used to confirm signal saturation. All ^{25}Mg shifts were referenced to 5 M $MgCl_2$(aq) at 0 ppm. ^2H MAS NMR experiments were performed at 116.7 MHz on a Bruker Avance III 7.02 Tesla (300 MHz) spectrometer with a 3.2 mm MAS probe. Deuterated diglyme (D; 98%, Cambridge Isotope Laboratories, Inc.) was introduced as a solvent to dissolve the Mg salt for ^2H MAS NMR measurement. All spectra were acquired with a rotor-synchronized echo pulse sequence, a $\pi/2$ pulse width of 4 μs, and a recycle delay of 0.2 s at a spinning speed of 15 kHz. All ^2H spectra were referenced to D_2O (98%) at 4.8 ppm.

Solutions were analyzed with a PerkinElmer Optima 8300DV ICP-OES. Standards for the ICP measurements were prepared from spectroscopic standard solutions procured from Ultra Scientific (North Kingstown, RI) and SPEX Certiprep (Metuchen, NJ). The samples were dissolved by KOH with KNO_3 fusion. Each sample was put in a Zr crucible with ∼2 g of KOH and 0.3 g of KNO_3. The Zr crucibles were heated at 360 °C in a shaking hot block digester for a minimum of 1.5 h. The Zr crucibles were then placed in a furnace and heated at 450 °C for 1 h. After heating in the furnace, the Zr crucibles were cooled, and then, some deionized water was added to the Zr crucible to aid in removing the fuseate from the crucible. The fuseate was quantitatively transferred to a 100 mL Teflon beaker with more deionized water and neutralized with 3−4 mL of concentrated HCl. Once the solution in the beaker was neutralized, 2 mL of more concentrated HCl was added to the beaker, and the beaker was heated on a hot plate at 220 °C for 30 min. The solution was allowed to cool and then quantitatively transferred to a 50 mL class A volumetric flask. Deionized water was used to bring the solution to volume.

X-ray absorption near edge structure (XANES) and extended X-ray absorption fine structure (EXAFS) measurements were performed at beamline 9-BM at the Advanced Photon Source, Argonne National Laboratory (ANL). X-ray absorption spectra were collected in a transmission mode through the pristine and electrochemically treated ex situ electrode materials. Energy was scanned by a double-crystal Si(111) monochromator that was detuned by 50%, and the incident and transmitted intensity were measured by gas ionization chambers.

V L-edge X-ray absorption spectroscopy (XAS) measurements were carried out by beamline 4-ID-C at the Advanced Photon Source (APS) at Argonne National Laboratory (ANL; Lemont, IL). The spectra were collected in a total electron yield (TEY) mode at room temperature under ultrahigh vacuum conditions (below 10^{-8} Torr). Contributions from visible light were carefully minimized before the acquisition, and all spectra were normalized to the current from freshly evaporated gold on a fine grid positioned upstream of the main chamber. The collected spectra were aligned by the beamline reference and a basic normalization.

X-ray photoelectron spectroscopy (XPS) was performed with a high-resolution monochromatic Al Kα X-ray source (15 eV, 25 mA emission current, VSW MX 170b Rowland circle monochromator) and a 150 mm concentric hemispherical analyzer with a multichannel detector (VSW Class 150) operated in a constant energy analyzer mode. The photoemission angle is normalized to the surface, and all core level spectra were calibrated to an aliphatic C 1s peak fitting component at 284.6 eV and were recorded with a pass energy of either 22 or 44 eV. The XPS peak fitting was performed using XPSPEAK (R.W.M. Kwok, v. 4.1, Hong Kong, China, http://xpspeak.software.informer.com/4.1/). Elemental fractions were determined from the integration of peak intensity.

Scanning transmission electron microscopy (STEM) imaging were performed on an aberration-corrected JEOL JEM-ARM200CF operated at 200 kV, with a maximum spatial resolution of ∼73 pm. High angle annular dark field (HAADF) images were acquired simultaneously using the corresponding detectors.

■ ASSOCIATED CONTENT

Supporting Information

The Supporting Information is available free of charge at https://pubs.acs.org/doi/10.1021/acs.chemmater.9b04206.

Thermal gravimetric analysis of the $Mg(TPFA)_2$ electrolyte, Rietveld refinement analysis, magnified X-ray diffractions, X-ray diffraction patterns of the synthesized spinel oxides, ^{25}Mg MAS NMR spectra of $MgCr_{0.4}V_{1.6}O_4$, elemental analysis by ICP-OES, potential versus capacity profiles of $MgCrVO_4$ harvested at 3.6 V, Cr K-edge spectra, ^{25}Mg MAS NMR spectra of the diamagnetic region, XPS of different states of $MgCrVO_4$, electrochemical test with $Mg(ClO_4)_2$ dissolved in propylene carbonate, and details of synthetic conditions (PDF)

■ AUTHOR INFORMATION

Corresponding Authors

Baris Key − *Argonne National Laboratory, Lemont, Illinois;* orcid.org/0000-0002-1987-1629; Email: bkey@anl.gov

John T. Vaughey − *Argonne National Laboratory, Lemont, Illinois;* orcid.org/0000-0002-2556-6129; Email: vaughey@anl.gov

Other Authors

Bob Jin Kwon − *Argonne National Laboratory, Lemont, Illinois*

Ka-Cheong Lau − *Argonne National Laboratory, Lemont, Illinois*

Haesun Park − *Argonne National Laboratory, Lemont, Illinois;* orcid.org/0000-0001-6266-8151

Yimin A. Wu − *Argonne National Laboratory, Lemont, Illinois, and University of Illinois at Chicago, Chicago, Illinois*
Krista L. Hawthorne − *Argonne National Laboratory, Lemont, Illinois*
Haifeng Li − *University of Illinois at Chicago, Chicago, Illinois*
Soojeong Kim − *Argonne National Laboratory, Lemont, Illinois*
Igor L. Bolotin − *University of Illinois at Chicago, Chicago, Illinois*
Timothy T. Fister − *Argonne National Laboratory, Lemont, Illinois;* orcid.org/0000-0001-6537-6170
Peter Zapol − *Argonne National Laboratory, Lemont, Illinois;* orcid.org/0000-0003-0570-9169
Robert F. Klie − *Argonne National Laboratory, Lemont, Illinois, and University of Illinois at Chicago, Chicago, Illinois*
Jordi Cabana − *Argonne National Laboratory, Lemont, Illinois, and University of Illinois at Chicago, Chicago, Illinois;* orcid.org/0000-0002-2353-5986
Chen Liao − *Argonne National Laboratory, Lemont, Illinois;* orcid.org/0000-0001-5168-6493
Saul H. Lapidus − *Argonne National Laboratory, Lemont, Illinois*

Complete contact information is available at: https://pubs.acs.org/10.1021/acs.chemmater.9b04206

Author Contributions

All authors have given approval to the final version of the manuscript.

Notes

The authors declare no competing financial interest.

■ ACKNOWLEDGMENTS

This work was supported by the Joint Center for Energy Storage Research, an energy innovation hub funded by the U.S. Department of Energy, Office of Science, Basic Energy Sciences. This research used the resources of the Advanced Photon Source, a U.S. Department of Energy (DOE) Office of Science user facility operated for the DOE Office of Science by Argonne National Laboratory under contract no. DE-AC02-06CH11357. This work is conducted at Argonne National Laboratory supported by the U.S. Department of Energy under contract no. DE-A02-06CH11357. ICP-OES analysis was performed by S. Naik of the Analytical Chemistry Laboratory, Argonne National Laboratory.

■ REFERENCES

(1) Canepa, P.; Sai Gautam, G.; Hannah, D. C.; Malik, R.; Liu, M.; Gallagher, K. G.; Persson, K. A.; Ceder, G. Odyssey of Multivalent Cathode Materials: Open Questions and Future Challenges. *Chem. Rev.* **2017**, *117*, 4287−4341.
(2) Mao, M.; Gao, T.; Hou, S.; Wang, C. A critical Review of Cathodes for Rechargeable Mg Batteries. *Chem. Soc. Rev.* **2018**, *47*, 8804−8841.
(3) Muldoon, J.; Bucur, C. B.; Gregory, T. Quest for Nonaqueous Multivalent Secondary Batteries: Magnesium and Beyond. *Chem. Rev.* **2014**, *114*, 11683−11720.
(4) Tutusaus, O.; Mohtadi, R.; Arthur, T. S.; Mizuno, F.; Nelson, E. G.; Sevryugina, Y. V. An Efficient Halogen-Free Electrolyte for Use in Rechargeable Magnesium Batteries. *Angew. Chem., Int. Ed.* **2015**, *54*, 7900−7904.
(5) Yoo, H. D.; Shterenberg, I.; Gofer, Y.; Gershinsky, G.; Pour, N.; Aurbach, D. Mg Rechargeable Batteries: An on-going Challenge. *Energy Environ. Sci.* **2013**, *6*, 2265−2279.
(6) Aurbach, D.; Lu, Z.; Schechter, A.; Gofer, Y.; Gizbar, H.; Turgeman, R.; Cohen, Y.; Moshkovich, M.; Levi, E. Prototype Systems for Rechargeable Magnesium Batteries. *Nature* **2000**, *407*, 724−727.
(7) Sun, X.; Bonnick, P.; Duffort, V.; Liu, M.; Rong, Z.; Persson, K. A.; Ceder, G.; Nazar, L. F. A High Capacity Thiospinel Cathode for Mg Batteries. *Energy Environ. Sci.* **2016**, *9*, 2273−2277.
(8) Canepa, P.; Bo, S.-H.; Sai Gautam, G.; Key, B.; Richards, W. D.; Shi, T.; Tian, Y.; Wang, Y.; Li, J.; Ceder, G. High Magnesium Mobility in Ternary Spinel Chalcogenides. *Nat. Commun.* **2017**, *8*, 1−8.
(9) Wustrow, A.; Key, B.; Phillips, P. J.; Sa, N.; Lipton, A. S.; Klie, R. F.; Vaughey, J. T.; Poeppelmeier, K. R. Synthesis and Characterization of $MgCr_2S_4$Thiospinel as a Potential Magnesium Cathode. *Inorg. Chem.* **2018**, *57*, 8634−8638.
(10) Liu, M.; Rong, Z.; Malik, R.; Canepa, P.; Jain, A.; Ceder, G.; Persson, K. A. Spinel Compounds as Multivalent Battery Cathodes: A Systematic Evaluation Based on ab Initio Calculations. *Energy Environ. Sci.* **2015**, *8*, 964−974.
(11) Levi, E.; Levi, M. D.; Chasid, O.; Aurbach, D. A Review on the Problems of the Solid State Ions Diffusion in Cathodes for Rechargeable Mg Batteries. *J. Electroceram.* **2009**, *22*, 13−19.
(12) Ling, C.; Zhang, R.; Arthur, T. S.; Mizuno, F. How General is the Conversion Reaction in Mg Battery Cathode: A Case Study of the Magnesiation of α-MnO_2. *Chem. Mater.* **2015**, *27*, 5799−5807.
(13) Zhang, R. G.; Yu, X. Q.; Nam, K. W.; Ling, C.; Arthur, T. S.; Song, W.; Knapp, A. M.; Ehrlich, S. N.; Yang, X. Q.; Matsui, M. α-MnO_2 as a Cathode Material for Rechargeable Mg Batteries. *Electrochem. Commun.* **2012**, *23*, 110−113.
(14) Sai Gautam, G.; Canepa, P.; Urban, A.; Bo, S.-H.; Ceder, G. Influence of Inversion on Mg Mobility and Electrochemistry in Spinels. *Chem. Mater.* **2017**, *29*, 7918−7930.
(15) Arthur, T. S.; Zhang, R.; Ling, C.; Glans, P.-A.; Fan, X.; Guo, J.; Mizuno, F. Understanding the Electrochemical Mechanism of K-αMnO_2 for Magnesium Battery Cathodes. *ACS Appl. Mater. Interfaces* **2014**, *6*, 7004−7008.
(16) Kim, C.; Phillips, P. J.; Key, B.; Yi, T.; Nordlund, D.; Yu, Y.-S.; Bayliss, R. D.; Han, S.-D.; He, M.; Zhang, Z.; Burrell, A. K.; Klie, R. F.; Cabana, J. Direct Observation of Reversible Magnesium Ion Intercalation into a Spinel Oxide Host. *Adv. Mater.* **2015**, *27*, 3377−3384.
(17) Kim, C.; Adil, A. A.; Bayliss, R. D.; Kinnibrugh, T. L.; Lapidus, S. H.; Nolis, G. M.; Freeland, J. W.; Phillips, P. J.; Yi, T.; Yoo, H. D.; Kwon, B. J.; Yu, Y.-S.; Klie, R.; Chupas, P. J.; Chapman, K. W.; Cabana, J. Multivalent Electrochemistry of Spinel $Mg_xMn_{3-x}O_4$ Nanocrystals. *Chem. Mater.* **2018**, *30*, 1496−1504.
(18) Bayliss, R. D.; Key, B.; Gautam, G. S.; Canepa, P.; Kwon, B. J.; Lapidus, S. H.; Dogan, F.; Adil, A. A.; Lipton, A. S.; Baker, P. J.; Ceder, G.; Vaughey, J. T.; Cabana, J. Probing Mg Migration in Spinel Oxides. *Chem. Mater.* **2019**, DOI: 10.1021/acs.chemmater.9b02450.
(19) Chen, T.; Sai Gautam, G.; Huang, W.; Ceder, G. First-Principles Study of the Voltage Profile and Mobility of Mg Intercalation in a Chromium Oxide Spinel. *Chem. Mater.* **2018**, *30*, 153−162.
(20) Tutusaus, O.; Mohtadi, R.; Singh, N.; Arthur, T. S.; Mizuno, F. Study of Electrochemical Phenomena Observed at the Mg Metal/Electrolyte Interface. *ACS Energy Lett.* **2016**, *2*, 224−229.
(21) Cabana, J.; Kwon, B. J.; Hu, L. Mechanisms of Degradation and Strategies for the Stabilization of Cathode−Electrolyte Interfaces in Li-Ion Batteries. *Acc. Chem. Res.* **2018**, *51*, 299−308.
(22) Lau, K.-C.; Seguin, T. J.; Carino, E. V.; Hahn, N. T.; Connell, J. G.; Ingram, B. J.; Persson, K. A.; Zavadil, K. R.; Liao, C. Widening Electrochemical Window of Mg Salt by Weakly Coordinating

Perfluoroalkoxyaluminate Anion for Mg Battery Electrolyte. *J. Electrochem. Soc.* **2019**, *166*, A1510−A1519.
(23) Pecher, O.; Carretero-González, J.; Griffith, K. J.; Grey, C. P. Materials' Methods: NMR in Battery Research. *Chem. Mater.* **2016**, *29*, 213−242.
(24) Lee, J.; Seymour, I. D.; Pell, A. J.; Dutton, S. E.; Grey, C. P. A Systematic Study of ^{25}Mg NMR in Paramagnetic Transition Metal Oxides: Applications to Mg-ion Battery Materials. *Phys. Chem. Chem. Phys.* **2017**, *19*, 613−625.
(25) Zeng, D.; Cabana, J.; Bréger, J.; Yoon, W.-S.; Grey, C. P. Cation Ordering in $Li[Ni_xMn_xCo_{(1-2x)}]O_2$-Layered Cathode Materials: A Nuclear Magnetic Resonance (NMR), Pair Distribution Function, X-ray Absorption Spectroscopy, and Electrochemical Study. *Chem. Mater.* **2007**, *19*, 6277−6289.
(26) Wang, H.; Senguttuvan, P.; Proffit, D. L.; Pan, B.; Liao, C.; Burrell, A. K.; Vaughey, J. T.; Key, B. Formation of MgO during Chemical Magnesiation of Mg-Ion Battery Materials. *ECS Electrochem. Lett.* **2015**, *4*, A90−A93.
(27) Jiang, M.; Key, B.; Meng, Y. S.; Grey, C. P. Electrochemical and Structural Study of the Layered, "Li-Excess" Lithium-Ion Battery Electrode Material $Li[Li_{1/9}Ni_{1/3}Mn_{5/9}]O_2$. *Chem. Mater.* **2009**, *21*, 2733−2745.
(28) Dogan, F.; Long, B. R.; Croy, J. R.; Gallagher, K. G.; Iddir, H.; Russell, J. T.; Balasubramanian, M.; Key, B. Re-entrant Lithium Local Environments and Defect Driven Electrochemistry of Li- and Mn-Rich Li-Ion Battery Cathodes. *J. Am. Chem. Soc.* **2015**, *137*, 2328−2335.
(29) Sa, N.; Kinnibrugh, T. L.; Wang, H.; Sai Gautam, G.; Chapman, K. W.; Vaughey, J. T.; Key, B.; Fister, T. T.; Freeland, J. W.; Proffit, D. L.; Chupas, P. J.; Ceder, G.; Bareno, J. G.; Bloom, I. D.; Burrell, A. K. Structural Evolution of Reversible Mg Insertion into a Bilayer Structure of V_2O_5-nH_2O Xerogel Material. *Chem. Mater.* **2016**, *28*, 2962−2969.
(30) Proffit, D. L.; Fister, T. T.; Kim, S.; Pan, B.; Liao, C.; Vaughey, J. T. Utilization of Ca K-Edge X-ray Absorption Near Edge Structure to Identify Intercalation in Potential Multivalent Battery Materials. *J. Electrochem. Soc.* **2016**, *163*, A2508−A2514.
(31) Lu, Y. R.; Hsu, H. H.; Chen, J. L.; Chang, H. W.; Chen, C. L.; Chou, W. C.; Dong, C. L. *Phys. Chem. Chem. Phys.* **2016**, *18*, 5203−5210.
(32) Yoo, H. D.; Jokisaari, J. R.; Yu, Y.-S.; Kwon, B. J.; Hu, L.; Kim, S.; Han, S.-D.; Lopez, M.; Lapidus, S. H.; Nolis, G. M.; Ingram, B. J.; Bolotin, I.; Ahmed, S.; Klie, R. F.; Vaughey, J. T.; Fister, T. T.; Cabana, J. Intercalation of Magnesium into a Layered Vanadium Oxide with High Capacity. *ACS Energy Lett.* **2019**, *4*, 1528−1534.
(33) Dogan, F.; Croy, J. R.; Balasubramanian, M.; Slater, M. D.; Iddir, H.; Johnson, C. S.; Vaughey, J. T.; Key, B. Solid State NMR Studies of Li_2MnO_3 and Li-Rich Cathode Materials: Proton Insertion, Local Structure, and Voltage Fade. *J. Electrochem. Soc.* **2014**, *162*, A235−A243.
(34) Paik, Y.; Grey, C. P.; Johnson, C. S.; Kim, J. S.; Thackeray, M. M. Lithium and Deuterium NMR Studies of Acid-Leached Layered Lithium Manganese Oxides. *Chem. Mater.* **2002**, *14*, 5109−5115.
(35) Fulmer, G. R.; Miller, A. J. M.; Sherden, N. H.; Gottlieb, H. E.; Nudelman, A.; Stoltz, B. M.; Bercaw, J. E.; Goldberg, K. I. NMR Chemical Shifts of Trace Impurities: Common Laboratory Solvents, Organics, and Gases in Deuterated Solvents Relevant to the Organometallic Chemist. *Organometallics* **2010**, *29*, 2176−2179.
(36) Hohenberg, P.; Kohn, W. Inhomogeneous Electron Gas. *Phys. Rev.* **1964**, *136*, B864−B871.
(37) Kresse, G.; Furthmüller, J. Efficient iterative schemes for ab initio total-energy calculations using a plane-wave basis set. *Phys. Rev. B* **1996**, *54*, 11169−11186.
(38) Blöchl, P. E. Projector augmented-wave method. *Phys. Rev. B* **1994**, *50*, 17953−17979.
(39) Perdew, J. P.; Burke, K.; Ernzerhof, M. Generalized Gradient Approximation Made Simple. *Phys. Rev. Lett.* **1996**, *77*, 3865−3868.
(40) Dudarev, S. L.; Botton, G. A.; Savrasov, S. Y.; Humphreys, C. J.; Sutton, A. P. Electron-energy-loss spectra and the structural stability of nickel oxide: An LSDA+U study. *Phys. Rev. B* **1998**, *57*, 1505−1509.
(41) Wang, L.; Maxisch, T.; Ceder, G. Oxidation energies of transition metal oxides within the GGA+U framework. *Phys. Rev. B* **2006**, *73*, 195107.
(42) Henkelman, G.; Jónsson, H. Improved tangent estimate in the nudged elastic band method for finding minimum energy paths and saddle points. *J. Chem. Phys.* **2000**, *113*, 9978−9985.
(43) Ong, S. P.; Wang, L.; Kang, B.; Ceder, G. Li−Fe−P−O2 Phase Diagram from First Principles Calculations. *Chem. Mater.* **2008**, *20*, 1798−1807.

https://dx.doi.org/10.1021/acs.chemmater.9b04206
Chem. Mater. 2020, 32, 1162−1171